Parameter Identification With PMUs for Instability Detection in Power Systems With HVDC Integrated Offshore Wind Energy

Lina He, *Student Member, IEEE*, and Chen-Ching Liu, *Fellow, IEEE*

***Abstract*—Large-scale offshore wind farms can be integrated with onshore ac grids by the voltage source converter based high voltage direct current (VSC-HVDC) technology. The resulting impact on the security of ac grids can be significant. Therefore, it is important to develop an HVDC model for online stability monitoring of the integrated ac/dc systems. This paper proposes a new HVDC model based on a circuit-theoretic foundation. With the available phasor measurement units (PMUs) at VSC stations, the parameters of the HVDC equivalent model can be identified in real-time by synchronized voltage and current phasor measurements at VSC ac terminals. The proposed HVDC model is applied to online voltage instability detection for integrated ac/dc systems by the Thevenin impedance matching. The HVDC equivalent circuit enables the Thevenin equivalent impedance of the HVDC-connected offshore wind farm to be determined directly from the PMU measurements. Numerical simulations are performed on the IEEE 39-bus system with an HVDC-connected offshore wind farm to validate the effectiveness of the proposed HVDC model.**

***Index Terms*—Offshore wind generators, phasor measurement unit (PMU), Thevenin equivalent, voltage instability detection, voltage source converter based high voltage direct current (VSC-HVDC).**

I. Introduction

WITH the anticipated high level penetration of offshore wind power, increasing voltage source converter based high voltage direct current (VSC-HVDC) connections are expected for wind power integration with onshore ac grids [1]. For analysis of the integrated ac/dc systems, it is important to develop the VSC-HVDC models for different time scales.

VSC-HVDC models have been reported in the literature for different types of analysis, including steady-state, transients, and dynamics, e.g., [2], [3]. In steady-state analysis, VSC-HVDC converters are viewed as ac voltage sources without consideration of dc dynamics and controls [4], [5]. The steady-state model is generally applied to power flow and optimal power flow analysis. The (electromagnetic) transient model of VSC-HVDC converters needs to demonstrate the detailed operating conditions of switches [6], [7]. It is used to assess the system response during disturbances in the short time scale, such as harmonics and dc fault transients, where detailed transient behavior is of importance. Dynamic analysis of VSC-HVDC converters is usually conducted by the average converter model that emphasizes on converter active and reactive power exchange with the ac grid to determine the corrective actions. The average converter model is represented by three parts, i.e., ac side phasor model, dc side dynamic model, and controllers [8], [9].

The time scale of power system dynamics ranges from milliseconds to minutes or even hours, including short-term and long-term dynamic phenomena. The period of interest for long-term stability extends from several seconds to several minutes or more. Slower acting devices need to be considered in long-term stability analysis, include tap-changing transformers, thermostatically controlled loads, and generator current limiters. Compared with those devices, the VSC-HVDC connection has a much faster dynamic response due to the pulse width modulation (PWM) technology. The typical response time of dc dynamics is in the order of milliseconds [10]. The existing VSC-HVDC dynamic models for stability analysis involve fast dc dynamics that can significantly increase the complexity of system models and the computation time for long-term, time domain dynamic simulations. Hence, it is not practical to use existing VSC-HVDC dynamic models for online long-term dynamic analysis.

With increasing installations of HVDC-connected offshore wind generators, stability studies of integrated ac/dc systems have become an important subject. It is important to develop a VSC-HVDC model that meets the accuracy and computational requirements for online analysis. To fill this gap, this paper proposes an HVDC equivalent model founded on circuit theory for the quasi steady-state (QSS) time scale. The QSS technique has been used extensively in long-term stability analysis [11], [12]. Based on decomposition of time scales, faster dc phenomena can be approximated by their equilibrium conditions during long-term stability analysis to reduce the complexity of system models [11]. The proposed VSC-HVDC QSS model is reduced to an equivalent "Γ" shaped circuit in this paper. Assuming the availability of PMUs, the parameters of this HVDC

Manuscript received March 14, 2013; revised June 21, 2013 and August 30, 2013; accepted September 05, 2013. Date of publication October 08, 2013; date of current version February 14, 2014. This work was supported by the EU project "Twenties," Transmission system operation with large penetration of Wind and other renewable Electricity sources in Networks by means of innovative Tools and Integrated Energy Solutions. Paper no. TPWRS-00311-2013.

L. He is with the School of Mechanical and Materials Engineering, University College Dublin, Belfield, Dublin 4, Ireland (e-mail: lina.he@ucdconnect.ie).

C.-C. Liu is with the School of Electrical Engineering and Computer Science, Washington State University, Pullman, WA 99164-2752 USA, and also with the School of Mechanical and Materials Engineering, University College Dublin, Belfield, Dublin 4, Ireland (e-mail: liu@ucd.ie).

Color versions of one or more of the figures in this paper are available online at http://ieeexplore.ieee.org.

Digital Object Identifier 10.1109/TPWRS.2013.2283656

equivalent model can be identified in real-time by PMU measurements from both VSC stations. During system operations, PMU data involves all dynamic information of VSCs on the ac side, including fast dynamics and controls that are reflected in the time-varying impedances of the HVDC equivalent circuit. Compared with existing HVDC dynamic models, the proposed PMU-based HVDC equivalent circuit greatly simplifies system models with no loss of dynamics of the VSC-HVDC link. Therefore, it is able to analyze long-term stability fast but accurately in an online environment. To the best of the authors' knowledge, the proposed PMU-based HVDC equivalent model has not been reported previously.

In this study, the proposed HVDC circuit model is applied to online voltage instability detection for ac grids with HVDC-connected offshore wind generators. The available PMU technology enables direct computation of the equivalent impedances of the HVDC system viewed from the offshore wind farm terminal and the point of common coupling (PCC). This HVDC equivalent circuit is used to explicitly determine the Thevenin impedance of HVDC-connected offshore wind generators. Based on the Thevenin impedance matching, it is able to perform online voltage instability detection of integrated ac/dc systems.

The existing Thevenin impedance matching methods use a "black box" method for identification of the Thevenin equivalent circuit. These methods use voltage and current phasors acquired at a local load bus to estimate the Thevenin equivalent parameters of the power grid viewed from this load bus [13]–[15]. A typical estimation method is to utilize the recursive least-squares method based on two or more consecutive measurement sets collected at this load bus [13]. This method implicitly assumes that the equivalent Thevenin parameters are constant during the interval between the two (or more) consecutive local measurement sets [16]. Singularity can arise in case the consecutive measurement sets do not change sufficiently. In addition, a large data window is needed to suppress possible system oscillations.

In contrast to the "black box" methods, the proposed explicit circuit model of the HVDC connection enables direct identification of the Thevenin equivalent impedance of an HVDC-connected offshore wind farm viewed from the PCC. Real-time voltage instability detection can be performed without the time delay needed to acquire consecutive sets of measurements in previous approaches. In addition, this paper presents a load shedding scheme as an application of the proposed HVDC equivalent circuit. This algorithm uses the Zbus method to determine the minimal load shedding for mitigation of voltage instability. It is noted, however, the proposed HVDC equivalent model is not intended for the analysis of short-term instability following large disturbances.

The organization of this paper is as follows. Section II derives the equivalent model of the VSC-HVDC link based on circuit theory by using the PMU technology. In Section III, it is applied to directly identify the Thevenin equivalent of HVDC-connected offshore wind generators for online voltage instability detection of integrated ac/dc systems. Section IV presents the load shedding algorithm based on the Zbus approach to determine the minimal load shedding. Numerical simulation results are reported in Section V to validate the effectiveness of the proposed HVDC equivalent model in voltage instability detection and control.

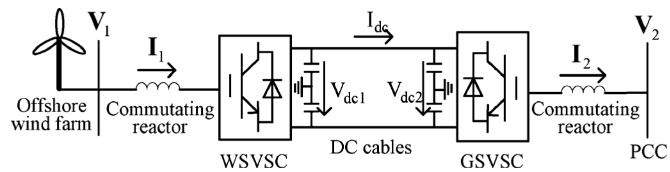

Fig. 1. VSC-HVDC connected offshore wind farm.

II. Equivalent Model of an HVDC-Connected Offshore Wind Farm

A. SSQ Model of VSC-HVDC Link

As shown in Fig. 1, a wind farm with doubly fed induction generators (DFIGs) is connected to an onshore ac grid through a point-to-point VSC-HVDC link. In the VSC-HVDC link, the wind farm VSC (WFVSC) regulates the magnitude and frequency of the WFVSC ac terminal voltage to enable the collection of wind power. The grid side VSC (GSVSC) controls the dc link voltage at a constant level and provides reactive power support for the onshore ac grid to maintain the PCC voltage at an expected level. The d,q-axis decoupling current controller is used to achieve independent control of active and reactive power. Detailed control configurations of the VSC-HVDC link for integration of offshore wind power are reported in [17].

Based on the PWM technology, VSCs can adjust the magnitude and phase angle of their ac side voltage fast to achieve independent control of active and reactive power. This allows VSCs to be modeled as controlled voltage sources for stability analysis of the ac grids. The dynamic equivalent circuit of a point-to-point VSC-HVDC (i.e., the average converter model) is shown in Fig. 2 [9]. This model has been widely used for stability analysis of ac/dc systems. It is noted that phasors (complex numbers) in this paper are bold-faced, while the magnitudes of phasors and dc variables are in plain symbols, i.e.,

$\mathbf{V}_1$	voltage phasor of WFVSC ac terminal;
$\mathbf{V}_2$	voltage phasor of GSVSC ac terminal (i.e., PCC);
$\mathbf{V'}_1$	AC side voltage phasor of WFVSC;
$\mathbf{V'}_2$	AC side voltage phasor of GSVSC;
$\mathrm{V}_{\mathrm{dc1}}$	DC side voltage of WFVSC;
$\mathrm{V}_{\mathrm{dc2}}$	DC side voltage of GSVSC;
$\mathbf{I}_1$	AC side current phasor of WFVSC;
$\mathbf{I}_2$	AC side current phasor of GSVSC;
I_{dc}	DC link current;
$\mathbf{Z}_1$	sum of WFVSC commutating reactor impedance and equivalent impedance of switch losses;
$\mathbf{Z}_2$	sum of GSVSC commutating reactor impedance and equivalent impedance of switch losses;
R_{dc}	resistance of dc cables.

As shown in Fig. 2, the dynamic elements of the dc circuit include capacitors and equivalent inductors of dc cables. The corresponding dynamic model is represented by differential equations. For VSC-HVDC systems, the typical response time of dc

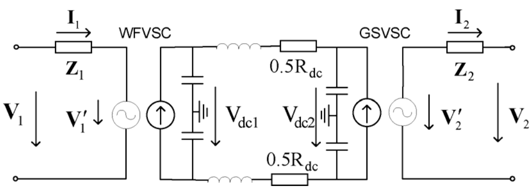

Fig. 2. Dynamic equivalent circuit of point-to-point VSC-HVDC link.

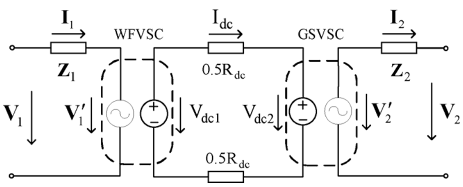

Fig. 3. QSS model of point-to-point VSC-HVDC link.

dynamics (in the order of milliseconds) is much shorter than the time scale of long-term stability. Therefore, fast dc dynamics are approximated by their equilibrium conditions in the proposed HVDC QSS model. DC capacitors are equivalent to voltage sources with identical steady-state voltages of the dc capacitors. The dc cable inductance is neglected as it is generally small. The resulting QSS model of the point-to-point VSC-HVDC is shown in Fig. 3. As noted, voltage sources in the QSS model are modeled to represent voltage characteristics of the terminals.

Assuming the dc voltage utilization related to the PWM mode is 1, the relationship between ac and dc side voltage magnitudes of the WFVSC and GSVSC can be written as

$$\mathrm{V'}_1 = \frac{\mathrm{M}_1}{\sqrt{2}}\mathrm{V}_{\mathrm{dc1}}, \quad \mathrm{V}'_2 = \frac{\mathrm{M}_2}{\sqrt{2}}\mathrm{V}_{\mathrm{dc2}} \tag{1}$$

where the symbols of M_1 and M_2 indicate the PWM modulation ratios of the WFVSC and GSVSC, respectively.

B. VSC-HVDC Equivalent Model Based on Circuit Theory

According to the terminal voltage characteristics of VSCs, VSCs can be viewed as special transformers. In a power system, the standard transformer circuit is modeled by an equivalent π-shaped network for simplification of calculations [18]. The derivation of the transformer equivalent circuit is based on the voltage-current relationship of the transformer terminals. The same concept is used here for derivation of the HVDC equivalent model.

As shown in Fig. 3, the dc link voltage equation is given by

$$\mathrm{V}_{\mathrm{dc1}} = \mathrm{I}_{\mathrm{dc}}\mathrm{R}_{\mathrm{dc}} + \mathrm{V}_{\mathrm{dc2}}. \tag{2}$$

According to (1) and (2), the GSVSC ac side voltage magnitude can be expressed as a function of the WFVSC ac side voltage magnitude. That is,

$$\mathrm{V'}_2 = \frac{\mathrm{M}_2}{\mathrm{M}_1}\mathrm{V'}_1 - \frac{\mathrm{M}_2}{\sqrt{2}}\mathrm{I}_{\mathrm{dc}}\mathrm{R}_{\mathrm{dc}}. \tag{3}$$

Therefore, using (3), the equivalent voltage source $\mathbf{V'}_2$ can be represented as the sum of equivalent voltage sources $(\mathrm{M}_2)/(\mathrm{M}_1)\mathrm{V'}_1\angle\delta_2$ and $-(\mathrm{M}_2)/(\sqrt{2})\mathrm{I}_{\mathrm{dc}}\mathrm{R}_{\mathrm{dc}}\angle\delta_2$ (where the symbol δ_2 indicates the phasor angle of $\mathbf{V'}_2$). The HVDC QSS model is simplified as a two-port network, which is shown in Fig. 4. The item of $(\mathrm{M}_2)/(\sqrt{2})\mathrm{I}_{\mathrm{dc}}\mathrm{R}_{\mathrm{dc}}$ in (3) corresponds to the equivalent voltage drop of the dc link viewed at the GSVSC ac terminal. By superposition, the equivalent voltage source of $(\mathrm{M}_2)/(\mathrm{M}_1)\mathrm{V'}_1\angle\delta_2$ is represented as the sum of equivalent voltage sources $(\mathrm{M}_2/\mathrm{M}_1)\mathrm{V'}_1\angle\delta_2 - \mathbf{V'}_1$ and $\mathbf{V'}_1$. The resulting equivalent circuit is shown in Fig. 5.

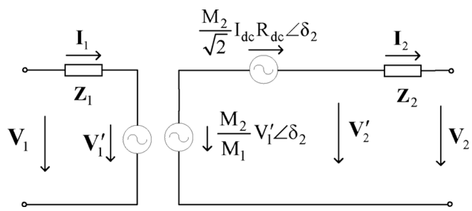

Fig. 4. Equivalent two-port network of point-to-point VSC-HVDC link.

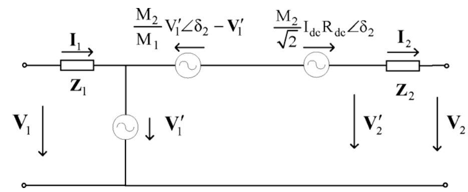

Fig. 5. Equivalent circuit of point-to-point VSC-HVDC link.

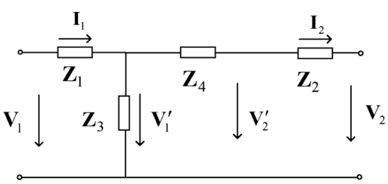

Fig. 6. Simplified equivalent circuit of point-to-point VSC-HVDC link.

The VSC-HVDC link is a passive network with equivalent voltage source branches as shown in Fig. 5. By the Substitution theorem in circuit theory, any branch in a passive network can be substituted by an impedance that maintains the identical voltage across and current through the branch. Hence, the circuit shown in Fig. 5 is equivalent to an impedance network with the identical voltage and current relationship of each corresponding branch, as shown in Fig. 6. The equivalent impedances in Fig. 6 are given by

$$\mathbf{Z}_3 = \frac{\mathbf{V'}_1}{\mathbf{I}_1 - \mathbf{I}_2}, \quad \mathbf{Z}_4 = \frac{\mathbf{V'}_1 - \frac{\mathrm{M}_2}{\mathrm{M}_1}\mathrm{V}_1\angle\delta_2 + \frac{\mathrm{M}_2}{2}\mathrm{I}_{\mathrm{dc}}\mathrm{R}_{\mathrm{dc}}\angle\delta_2}{\mathbf{I}_2}. \tag{4}$$

The symbol of $\mathbf{Z}_1$ represents the sum of the WFVSC commutating reactor impedance and equivalent impedance of switch losses. Its voltage drop is much lower than the ac side voltage magnitude of the WFVSC,$\mathrm{V'}_1$. Therefore, for simplification, the branch of $\mathbf{Z}_3$ can be moved forward. As a result, the point-to-point HVDC model is reduced to a "Γ" shaped circuit, as shown in Fig. 7. The impedances $\mathbf{Z}_{\mathrm{E1}}$ and $\mathbf{Z}_{\mathrm{E2}}$ are defined by

$$\mathbf{Z}_{\mathrm{E1}} = \mathbf{Z}_3, \quad \mathbf{Z}_{\mathrm{E2}} = \mathbf{Z}_1 + \mathbf{Z}_4 + \mathbf{Z}_2. \tag{5}$$

C. PMU-Based Parameter Identification for VSC-HVDC Equivalent Circuit

Based on the availability of PMUs at both VSC stations, the voltage and current phasor measurements of VSC ac terminals

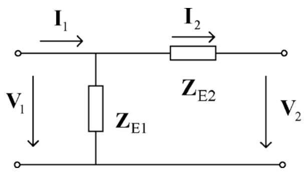

Fig. 7. "Γ" shaped equivalent circuit of point-to-point VSC-HVDC link.

can be obtained at the center station. By Kirchhoff's law, the equivalent impedances $\mathbf{Z}_{E1}$ and $\mathbf{Z}_{E2}$ are determined in real-time by the synchronized phasor measurements, i.e., $\mathbf{V}_1$, $\mathbf{I}_1$, $\mathbf{V}_2$ and $\mathbf{I}_2$. Their expressions are given by

$$\mathbf{Z}_{E1} = \frac{\mathbf{V}_1}{\mathbf{I}_1 - \mathbf{I}_2}, \quad \mathbf{Z}_{E2} = \frac{\mathbf{V}_1 - \mathbf{V}_2}{\mathbf{I}_2}. \tag{6}$$

The sampling rate of PMUs can be up to 10 000 points per second, i.e., 200 points per cycle for a 50-Hz system and its typical data transfer rate is 20 ms per packet. Therefore, equivalent impedances of the proposed HVDC circuit can be updated every 20 ms. During power system operation, real-time PMU measurements reflect the effects of fast HVDC controls through the time-varying voltages and currents on the VSC ac side. These time-varying voltage and current phasors are applied to determine equivalent impedances of the proposed HVDC equivalent circuit. In other words, the VSC-HVDC dynamics, including fast HVDC controls, are not modeled explicitly but their effects will be reflected in the time-varying impedances of the HVDC equivalent circuit.

In actual power systems, PMU measurements need to be transmitted from the VSC stations to a control center. Typical communication links include fiber-optic cables, digital microwave links and power lines. For any media, the data communication delays exist. Currently, the communication delay associated with fiber-optic cables is about 20–100 ms [19]. Since the time scale of voltage stability ranges from seconds to minutes, the communication time delay associated with fiber-optic cables is acceptable for the long-term voltage instability detection. As the reliability of data transmission is significant for online stability monitoring, the communication links must be redundant.

D. Discussion of HVDC Equivalent Circuit

When a voltage dip occurs at the PCC, the GSVSC current can increase to its rating. The PCC voltage reduction decreases the power transmission capability of the GSVSC. As the WFVSC power injections from DFIGs cannot be reduced instantaneously, the unbalanced power in the HVDC link leads to charging of dc capacitors. As a result, the dc link can experience a severe overvoltage. This in turn increases the WFVSC ac terminal voltage, $\mathbf{V}_1$. During this period, the GSVSC ac side current, $\mathbf{I}_2$, keeps at its limit. By (6), it is obtained that the HVDC Thevenin impedances $\mathbf{Z}_{E2}$ is increased as a response to the PCC voltage decline. At this moment, the reaction of the Thevenin impedance $\mathbf{Z}_{E1}$ depends on the WFVSC ac side current, $\mathbf{I}_1$. In case the WFVSC ac side current reaches its rating due to its power regulation capability, the HVDC Thevenin impedances $\mathbf{Z}_{E1}$ will rise with the increasing WFVSC ac terminal voltage.

In the proposed HVDC circuit, equivalent impedances vary with time based on PMU measurements. The time-varying impedances incorporate the effects of HVDC controls that are significant for the ac grids due to the high capability of the VSC power regulation. Therefore, the PCC cannot be modeled simply as a PV-node. The proposed PMU-based HVDC equivalence method can also be applied to multi-HVDC connections. As an example, the equivalent circuit of an H-shaped VSC-HVDC connection is derived and the results are given in Appendix A.

III. Thevenin Equivalent of an HVDC-Connected Offshore Wind Farm and Its Applications

A report from European Wind Energy Association (EWEA) indicates that the installation capacity of EU offshore wind units will be increased to 150 GW by 2030 as additional generation resources to meet 14% of the EU electricity demand [1]. With increasing penetration of the offshore wind power, it is important to evaluate its impact on system stability of ac power grids. Generally, offshore wind farms are large-scale, up to several GWs. A loss of large-scale offshore wind generations will cause a significant deficit on the ac power grids that may induce severe voltage and frequency stability problems. Furthermore, VSC-HVDC connections provide effective active and reactive power controls for the ac power grids. Therefore, it is essential to consider the HVDC-connected offshore wind farms as an integral part of the future integrated ac/dc systems.

As power systems are operated closer to their transmission limits, voltage instability has become a cause of widespread power outages. As mentioned, existing voltage instability detection using the Thevenin impedance matching is mainly based on a "black box" approach. In contrast, the proposed HVDC circuit model enables the Thevenin impedance of HVDC-connected offshore wind generators to be accurately and directly determined for online voltage instability detection.

A. Thevenin Equivalent of an HVDC-Connected Offshore Wind Farm

In power system analysis, wind farms with DFIGs can be aggregated into an equivalent wind turbine to reduce the model dimension and complexity [20]. The accuracy of the dynamic aggregated model is validated by comparing simulations based on contingency analysis [21]. The aggregation of wind turbines is based on the assumption that all turbines in an offshore wind farm can be represented by an equivalent wind turbine. The impedance and electromotive force of the aggregated wind generator change over time, but slowly. Therefore, it is reasonable to use the transient impedance and transient electromotive force to simplify the aggregated wind generator model for stability analysis. In addition, the wind turbine collector system and pad-amounted transformer need to be considered in the aggregation of offshore wind farms. Identification of these equivalent parameters can be found in [22].

Using the "Γ" shaped HVDC equivalent model, the HVDC-connected offshore wind farm is represented as the circuit in Fig. 8. The offshore wind farm based on DFIGs is represented by the dynamic model of an integrated generator [23]. The symbols of $\mathrm{r_s}$ and $\mathrm{X'}$ correspond to the stator resistance and transient

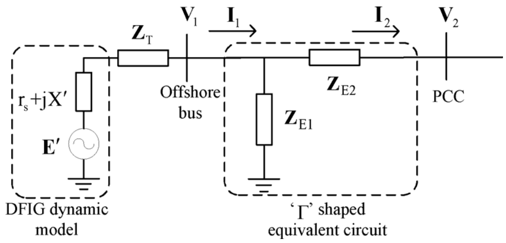

Fig. 8. Equivalent circuit of an HVDC-connected offshore wind farm.

reactance of DFIGs, respectively. The transient reactance is determined by

$$\mathrm{X}' = \omega_s \frac{\mathrm{L}_{ss} - \mathrm{L}_m^2}{\mathrm{L}_{rr}} \tag{7}$$

where ω_s is the synchronous speed, L_m is the mutual inductance between rotor and stator windings, and L_{ss} and L_{rr} are the self inductances of rotor and stator windings, respectively. The symbol of $\mathbf{Z}_T$ represents the sum of equivalent impedances from the cable collector system, pad-amounted transformer, and station step-up transformer.

The equivalent circuit of the HVDC-connected offshore wind farm can be transformed into a Thevenin equivalent circuit. The Thevenin equivalent impedance is given by

$$\mathbf{Z}_{th} = \frac{(r_s + j\mathrm{X}' + \mathbf{Z}_T) * \mathbf{Z}_{E1}}{r_s + j\mathrm{X}' + \mathbf{Z}_T + \mathbf{Z}_{E1}} + \mathbf{Z}_{E2}. \tag{8}$$

Using the available PMU measurements at VSC ac terminals, the Thevenin equivalent impedance viewed at the PCC can be calculated in real-time by substituting (6) and (7) into (8).

The Thevenin equivalent impedance is equal to the sum of $(r_s + j\mathrm{X}' + \mathbf{Z}_T)//\mathbf{Z}_{E1}$ and $\mathbf{Z}_{E2}$. The value of $(r_s + j\mathrm{X}' + \mathbf{Z}_T)//\mathbf{Z}_{E1}$ is smaller than that of $(r_s + j\mathrm{X}' + \mathbf{Z}_T)$ due to the parallel connection. As shown in (5), the impedance $\mathbf{Z}_{E2}$ is the sum of $\mathbf{Z}_1$, $\mathbf{Z}_2$ and $\mathbf{Z}_4$. The symbols $\mathbf{Z}_1$ and $\mathbf{Z}_2$ represent the sum of the WFVSC and GSVSC commutating reactor impedance and equivalent impedance of switch losses, respectively. The symbol $\mathbf{Z}_4$ is the equivalent impedance representing the losses of dc cables. The impedance $\mathbf{Z}_{E2}$ represents the transmission loss of the HVDC link. In an integrated ac/dc system, the offshore wind farm is usually far from the onshore grid, say, over 100 km. Compared with other devices, e.g., step-up transformers, losses on the dc link loss is much more significant, i.e., $(r_s + j\mathrm{X}' + \mathbf{Z}_T) \ll \mathbf{Z}_{E2}$. Therefore, the Thevenin impedance of the HVDC-connected offshore wind farm mainly depends on the HVDC equivalent parameter $\mathbf{Z}_{E2}$ that is not related to the wind farm.

B. Voltage Instability Detection Using Thevenin Impedance Matching

The HVDC-connected offshore wind farm is connected to an ac grid. This integrated ac/dc grid has a Thevenin equivalent circuit as shown in Fig. 9. The PCC and ac grid are viewed as a virtual "load" bus and lumped load, respectively. Based on the maximal power transfer theorem, the power output of the Thevenin equivalent source is maximized when the Thevenin and load impedances are identical in magnitude [14], i.e.,

$$|\mathbf{Z}_{th}| = |\mathbf{Z}_{load}|. \tag{9}$$

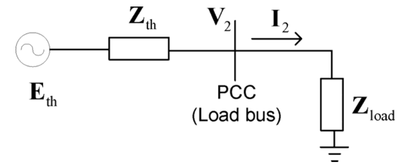

Fig. 9. Thevenin equivalent circuit of an integrated ac/dc grid.

During the system operation, the maximal power transfer of a power grid corresponds to the point of voltage collapse. Therefore, the difference between the load and Thevenin impedance magnitudes, i.e., $|\mathbf{Z}_{load}| - |\mathbf{Z}_{th}|$, can be used to determine the proximity of the operating point to a voltage collapse, i.e., a voltage stability margin. The Thevenin impedance matching method is extended in this paper for study of voltage instability detection for an integrated ac/dc system. The lumped load impedance can be directly determined by the voltage and current phasor measurements viewed at the PCC, i.e.,

$$\mathbf{Z}_{load} = \frac{\mathbf{V}_2}{\mathbf{I}_2}. \tag{10}$$

Based on the explicit model of the HVDC-connected offshore wind farm, both the Thevenin and load impedances seen at the PCC can be directly calculated with synchronized phasor measurements available at VSC ac terminals. The Thevenin impedance matching using the proposed HVDC equivalent circuit effectively overcomes drawbacks of local approaches, such as extended time delays and singularity conditions in computation.

C. Other Applications of the Proposed HVDC Equivalent Circuit

The proposed HVDC equivalent circuit simplifies the system model and improves the computational efficiency for time domain simulations. It is derived from the HVDC QSS model for long-term stability analysis of integrated ac/dc systems. The electromagnetic transients are beyond the scope of the proposed model. Section III-B discusses its application to voltage instability detection using the Thevenin impedance matching. Besides voltage instability detection, there are other important applications. For example,

1) Long-term frequency stability analysis. The time scale of long-term frequency stability ranges from seconds to several minutes and involves devices such as prime mover systems and load voltage regulators [24]. Long-term frequency instability can be caused by steam turbine overspeed control or boiler/reactor protection. With consideration of those slow acting devices, the proposed HVDC equivalent circuit can be applied to long-term frequency analysis for integrated ac/dc grids.
2) Fault location. The Zbus approach is well known for the fault analysis of ac systems [25]. When an ac grid experiences a three-phase short circuit, the Zbus matrix with voltage measurements can be applied to identify the fault location. Using the proposed HVDC equivalent model, an integrated ac/dc system is transformed into an equivalent ac system. The Zbus matrix of the equivalent ac system can be obtained and utilized for the fault location of three-phase short circuit faults.

3) Load shedding. The Zbus matrix of the integrated ac/dc system is used in Section IV to determine the minimal load shedding for mitigation of voltage instability. In power systems, long-term voltage instability is usually caused by equipment outages, rather than initial disturbances [24]. The most common instability scenarios result from the loss of long-term equilibria, e.g., system load exceeds the capability of the generation and transmission systems. The cascading failure scenarios discussed in Section V serve as examples.

IV. Load Shedding Scheme to Mitigate Voltage Instability

A. Load Shedding Algorithm

In power grids, load shedding is the most common and effective last-resort remedial control to mitigate voltage instability. Its activation is designed to prevent the occurrence of a voltage collapse. The voltage stability margin may rapidly decline when the system operating point is close to the edge of a voltage collapse. Therefore, load shedding should be activated before the voltage stability margin actually drops to zero. In addition, the unavoidable communication delay of PMU data transmission needs to be considered. A safety margin $\delta_{\rm m}$ is specified to allow timely activation of load shedding. The safety margin can be pre-determined by offline system analysis.

Within the voltage stability limit, the safety margin is likely to be violated temporarily (i.e.,$0 < |\mathbf{Z}_{\rm load}| - |\mathbf{Z}_{\rm th}| < \delta_{\rm m}$, "warning area") during disturbances, such as system oscillations or element failures. After the appropriate damping adjustment or fault clearance, the system may be steered away from the warning area. To avoid a premature load shedding in these cases, this paper proposes a load shedding algorithm based on the analysis of the impedance magnitude ratio derivative $d(|\mathbf{Z}_{\rm th}|/|\mathbf{Z}_{\rm load}|)/dt$.

The variables of $\mathbf{Z}_{\rm th}$ and $\mathbf{Z}_{\rm load}$ are identified in real-time by synchronized phasor measurements available at the VSC ac terminals. The backward difference method is applied to determine $d(|\mathbf{Z}_{\rm th}|/|\mathbf{Z}_{\rm load}|)/dt$ at each sampling interval. When the voltage stability margin enters the warning area, say, at the ith sampling, the current $d(|\mathbf{Z}_{\rm th}|/|\mathbf{Z}_{\rm load}|)/dt$ is compared with that of the last sampling, i.e., the $({\rm i}-1)$th. An increased $d(|\mathbf{Z}_{\rm th}|/|\mathbf{Z}_{\rm load}|)/dt$ demonstrates that the present available adjustments are not sufficient to counteract the voltage decline. System voltages will be further reduced, leading to a possible voltage collapse. As the last resort action, load shedding can be activated to increase the voltage stability margin. To drive the voltage stability margin of this system away from the warning area, the expected increase of $|\mathbf{Z}_{\rm load}|$ achieved by load shedding can be represented as

$$\Delta|\mathbf{Z}_{\rm load}|_{\rm i} = (1+\alpha) * [\delta_{\rm m} - (|\mathbf{Z}_{\rm load}|_{\rm i} - |\mathbf{Z}_{\rm th}|_{\rm i})] \tag{11}$$

where α is a load shedding margin factor.

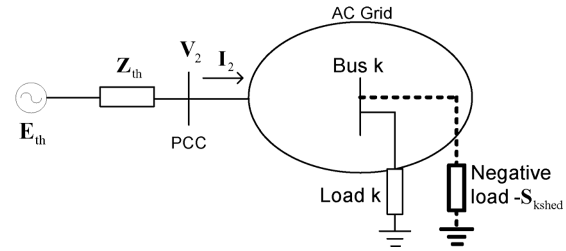

Fig. 10. Equivalent integrated ac/dc network with load shedding.

B. Minimal Load Shedding Strategy

The Zbus approach is applied to determine the minimal load shedding. As discussed in Section III-A, the Thevenin equivalent of the HVDC-connected offshore wind grid can be determined in real-time based on the PMU measurements. This Thevenin equivalent branch is used to modify the Zbus matrix of the integrated ac/dc system. When load shedding is activated at a load bus of the ac grid, say bus k, with the amount of $\mathbf{S}_{\rm kshed}$, it is viewed as a negative load with the identical amount to bus k, i.e., $-\mathbf{S}_{\rm kshed}$, as shown in Fig. 10. Its equivalent load impedance can be written as

$$\mathbf{Z}_{\rm kshed} = \mathbf{V}_{\rm k}^2/-\mathbf{S}_{\rm kshed}^* \tag{12}$$

where $\mathbf{V}_{\rm k}$ is the voltage phasor measurement on bus k.

Applying system node voltage equations, the resulting increase of the equivalent load impedance viewed at the PCC by load shedding at bus k is given by

$$\Delta\mathbf{Z}_{\rm load} = -\frac{\mathbf{Z}_{\rm PCCk} * \mathbf{V}_k/\mathbf{I}_2}{\mathbf{Z}_{\rm kk} + \mathbf{Z}_{\rm kshed}} \tag{13}$$

where $\mathbf{Z}_{\rm PCCk}$ is the transfer impedance between the PCC and bus k before load shedding, $\mathbf{I}_2$ is the measured current at the PCC, and $\mathbf{Z}_{\rm kk}$ denotes the impedance corresponding to bus k before load shedding.

To meet the required $\Delta|\mathbf{Z}_{\rm load}|_{\rm i}$ in (11), the expected load shedding amount at bus k is identified by solving simultaneous functions (11), (12) and (13); that is, see (14) at the bottom of the page.

This method is applied to calculate the load shedding amount at each load bus that meets the required $\Delta|\mathbf{Z}_{\rm load}|_{\rm i}$ in (11). By ranking the active power amount of load shedding at each load bus, the minimal load shedding amount and location can be determined. An example is shown in Section V-C. Due to its low computational requirement, this method is promising for the online environment.

V. Case Studies

A. Simulation System

As shown in Fig. 11(a) and (b), an offshore wind farm is connected to bus 23 of the IEEE 39-bus system through a

$$\mathbf{S}_{\rm kshed} = \left(\frac{{\rm V}_{\rm k}^2 * (\Delta|\mathbf{Z}_{\rm load}|_{\rm i}\angle\arg(\mathbf{V}_2/\mathbf{I}_2))}{\mathbf{Z}_{\rm PCCk} * \mathbf{V}_{\rm k}/\mathbf{I}_2 + \mathbf{Z}_{\rm kk} * (\Delta|\mathbf{Z}_{\rm load}|_{\rm i}\angle\arg(\mathbf{V}_2/\mathbf{I}_2))}\right)^* \tag{14}$$

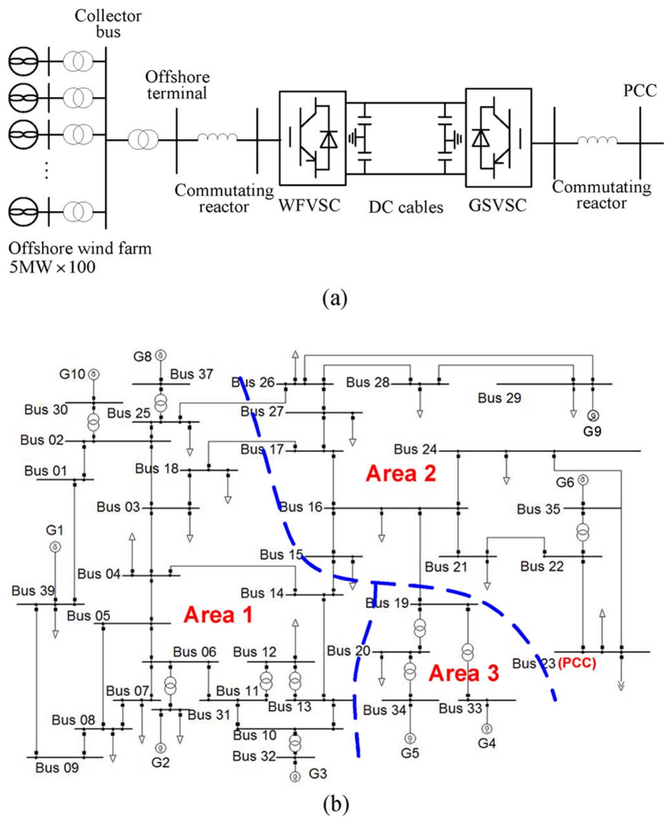

Fig. 11. IEEE 39-bus system with HVDC-connected offshore wind farm. (a) HVDC-connected offshore wind farm. (b) IEEE 39-bus system.

point-to-point two-level VSC-HVDC link. The VSC-HVDC link consists of two 600 MV, $\pm 150/132$ kV VSCs. The two-level average model of the VSC-HVDC connection is developed in DIgSILENT software tool. Its control mode has been discussed in Section II-A. The reactive power capability of the simulated VSCs ranges from -300 MVar (absorbing) to $+300$ MVar (sending). The commutating reactance of each VSC is 35 mH and dc capacitors connecting the positive pole and negative pole in the dc grid are 160 μF. The length of two XLPE dc cables is 100 km. The offshore wind farm is composed of 100 standard DFIGs, each rated at 5 MW. As shown in Fig. 11(a), DFIGs are connected to the collector bus through step-up transformers. The DFIG model has been well reported [23], [26]. The simulated DFIG dynamic model includes the wind turbine, induction generator, power electronic dc link, control system, and DFIG protection circuit. All DFIGs have identical parameters as shown in Appendix B.

The dynamic model of this integrated ac/dc system is developed in DIgSILENT PowerFactory on a 100 MVA base for time-domain simulations. Transmission lines of the IEEE 39-bus system rated at 1.5 kA are operated at a nominal voltage of 345 kV. The synchronous generator G2 serves as the reference machine. Induction motor loads account for 50% of the system load [27]. It is noted that a simple collector bus of offshore wind turbines is modeled in the simulation case to reduce the computational burden.

TABLE I
EVENT LIST OF CASCADING FAILURES

Lines	Events
line 22-23	At 5 s, initiate a three phase short circuit fault, and at 5.15 s, line 22-23 is cleared
line 21-22	Highly loaded and isolated at 10 s due to protection malfunction
line 16-19	Overloaded and isolated at 15 s
line 14-15	Overloaded and isolated at 20 s
line 17-18	Overloaded and isolated at 25 s
line 25-26	Overloaded and isolated at 30 s

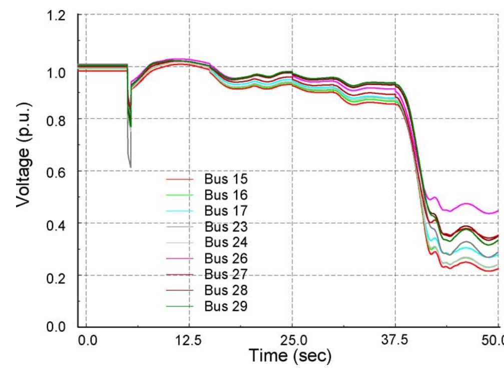

Fig. 12. Voltages at area 2 in IEEE 39-bus system.

B. Voltage Instability Detection

A voltage collapse case induced by cascading failures is simulated on the integrated ac/dc system to validate the proposed HVDC equivalent model for voltage instability detection. The cascading events are listed in Table I. In realistic systems, the time interval of two consecutive events can range from seconds to minutes. For the simulation purpose, the time interval between two consecutive events in the cascading sequence is 5 s.

With the isolation of line 25–26, the integrated ac/dc system is split into three islands, as shown in Fig. 11(b). Generation units in area 2, including offshore DFIGs, need to increase their active power output to meet the load requirements. The increased power transfer requires more reactive power to maintain the area 2 voltages at the expected levels. When area 2 generation units exhaust their reactive power reserve, PV-nodes behave as PQ-nodes. The resulting voltage declines further aggravate the generation deficit, leading to a voltage collapse. The area 2 voltages during cascading events are shown in Fig. 12.

The integrated ac/dc system is equivalent to a Thevenin circuit with the PCC as a virtual load bus. It is assumed that both VSC stations are installed with PMUs to acquire real-time measurements of voltage and current phasors at the VSC ac terminals. The voltage and current phasors of the VSC ac terminals during the simulation in DIgSILENT are transferred to MATLAB to identify the Thevenin and load impedances viewed at the PCC in real-time. Voltage instability detection is achieved by comparing the synchronized load and Thevenin impedance magnitudes.

The Thevenin and load impedances seen at the PCC are shown in Fig. 13. Both impedance curves have a similar trend before the isolation of line 25–26. After the system is split at 30 s, the Thevenin impedance dramatically increases with a sharp decline of the load impedance. Finally, the Thevenin

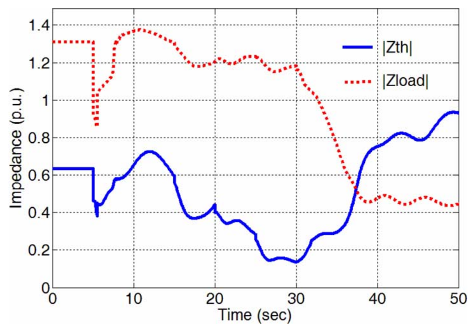

Fig. 13. Equivalent Thevenin and load impedance magnitudes viewed at PCC.

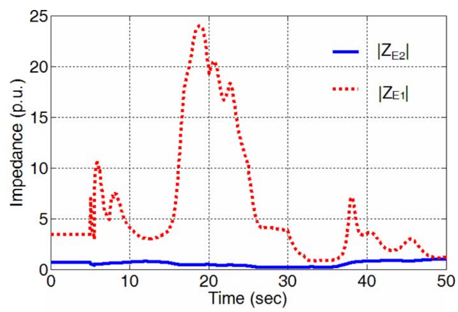

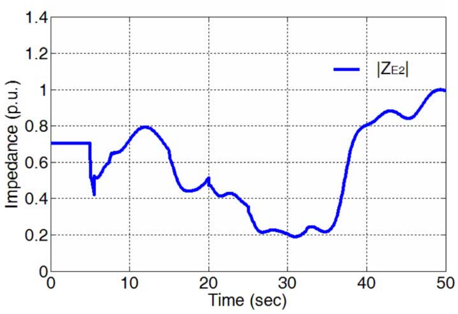

Fig. 14. (a) Magnitude curves of HVDC equivalent parameters during cascading events. (b) Zoomed-in curve of magnitude of $\mathbf{Z}_{\mathrm{E2}}$.

impedance curve intersects with the apparent load impedance curve at 38 s. This time is well matched with the voltage collapse point of area 2 shown in Fig. 12. It demonstrates that the proposed equivalent model can accurately reflect the HVDC dynamics during the system operation.

The computed magnitudes of HVDC equivalent parameters $\mathbf{Z}_{\mathrm{E1}}$ and $\mathbf{Z}_{\mathrm{E2}}$ are shown in Fig. 14(a). It is seen that the magnitude of $\mathbf{Z}_{\mathrm{E1}}$ is much larger than that of $\mathbf{Z}_{\mathrm{E2}}$ before the voltage collapse. The zoomed-in curve of the magnitude of $\mathbf{Z}_{\mathrm{E2}}$ is shown in Fig. 14(b). By comparing Figs. 13 and 14(b), it is found that the Thevenin impedance mainly depends on the HVDC equivalent parameter $\mathbf{Z}_{\mathrm{E2}}$, which is matched with the analysis in Section III-A. Therefore, this parameter can be used to estimate the Thevenin equivalent impedance magnitude viewed at the PCC to quickly determine the voltage instability margin of the integrated ac/dc system.

C. Load Shedding for Voltage Collapse Mitigation

Analysis of the system stability is performed on the IEEE 39 bus system with an HVDC-connected offshore wind farm for

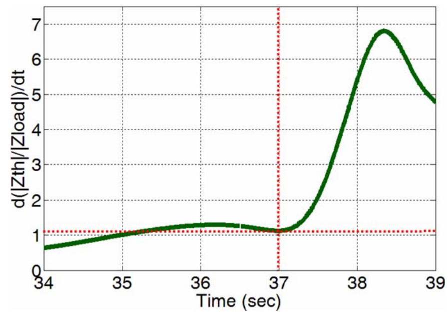

Fig. 15. Derivative of the impedance magnitude ratio $(d(|\mathbf{Z}_{\mathrm{th}}|/|\mathbf{Z}_{\mathrm{load}}|)/dt)$.

TABLE II
LOAD SHEDDING RANKING

Bus No.	Active power amount of expected load shedding (p.u.)	Actual active load (p.u.)
21	2.095	3.74
15	2.458	3.20
16	2.542	3.29
24	2.569	3.08
…	…	…

the determination of the safety margin δ_{m}. It is set as 0.2 p.u. in this study case and the applied load shedding margin factor is 30%.

For the simulation results shown in Fig. 13, the derivative of the impedance magnitude ratio $(d(|\mathbf{Z}_{\mathrm{th}}|/|\mathbf{Z}_{\mathrm{load}}|)/dt)$ is determined by the backward difference method. Its zoomed-in figure is shown in Fig. 15. The difference between the load and Thevenin equivalent impedance magnitudes in Fig. 13 is reduced to 0.2 p.u. at 36.6 s. At this moment, the voltage stability margin of the integrated ac/dc system enters the warning area. It is seen in Fig. 15 that the derivative of the impedance ratio performs a downward trend until 37 s. This is caused by system adjustments to steer the operating point back to a normal condition. After the available adjustment options are exhausted, the derivative of the impedance magnitude ratio dramatically increases, leading to a voltage collapse.

For the proposed algorithm, load shedding is activated at 37 s to increase the voltage stability margin and restore the system voltages. The expected increase of the lumped load impedance viewed at the PCC is 0.136 p.u., which is determined by (11). To meet this requirement, the load shedding amount on each load bus is calculated individually. Results ranked by the active power amount of load shedding are shown in Table II.

It is seen in Table II that the minimal required load shedding amount on bus 21 is less than the actual active load connected to bus 21. Therefore, the minimal load shedding amount in this simulation is determined by

$$\mathrm{S}_{\mathrm{minshed}} = (1 + \tan\varphi_{21}) * 2.095 = 2.095 + \mathrm{j}1.036$$

where φ_{21} is the power angle of load 21. After the activation of load shedding on bus 21 at 37 s, the system voltages are successfully restored, as shown in Fig. 16(a). The Thevenin and load impedances viewed at the PCC are shown in Fig. 16(b). This load shedding effectively prevents the Thevenin and load impedances from approaching each other. The voltage stability

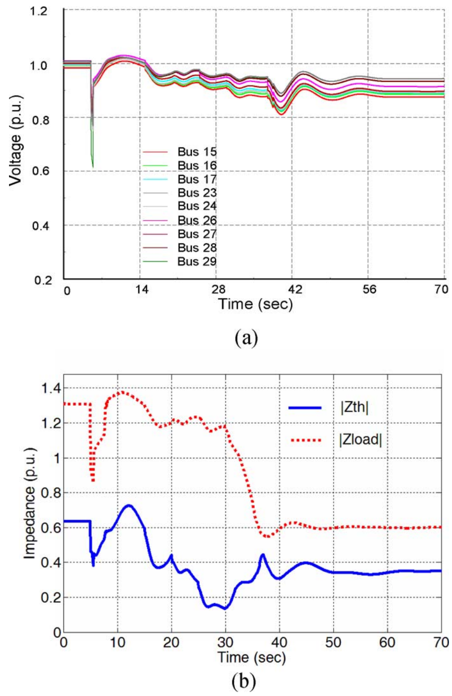

Fig. 16. System dynamics after load shedding: (a) voltage curves at area 2; (b) equivalent Thevenin and load impedance magnitudes viewed at PCC.

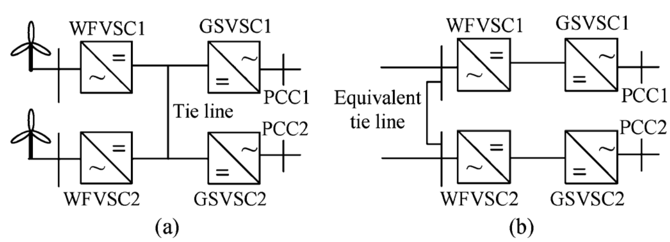

Fig. 17. (a) Integrated ac/dc system. (b) Integrated ac/dc system with equivalent tie line.

margin is maintained at about 0.25 p.u., which meets the safety margin requirement.

VI. Conclusion

This paper proposes an equivalent circuit of the point-to-point VSC-HVDC link based on circuit theory. It uses the QSS approximation for the purpose of long-term dynamic analysis. The application of the PMU technology enables the HVDC equivalent circuit to be calculated directly. The HVDC equivalent circuit is applied to online voltage instability detection and load shedding for mitigation of voltage collapse. Due to the limitation of the time scale, the proposed HVDC model is not intended for short-term instability studies. As an extension, the equivalent circuit of an H-shaped VSC-HVDC connection is also developed for the QSS time scale.

Appendix

A. Equivalent Circuit of H-Shaped VSC-HVDC

Fig. 17(a) illustrates an example multi-terminal HVDC grid for the integration of offshore wind farms. The power-voltage droop control is used to shift power between two point-to-point HVDC links through the dc tie line. The H-shaped HVDC can

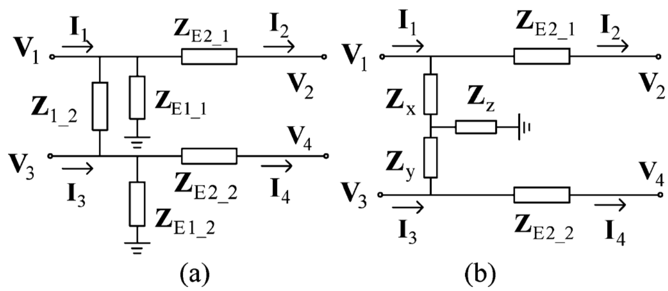

Fig. 18. Equivalent circuit of integrated ac/dc system with equivalent tie line.

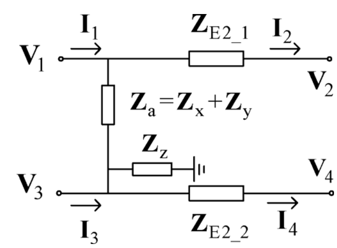

Fig. 19. Simplified equivalent circuit of integrated ac/dc system with equivalent tie line.

be viewed as a four-port network. Without changing the port characteristics of multi-HVDC, the dc tie line can be moved to the ac sides of WFVSCs with an equivalent impedance for the power shift. The resulting multi-HVDC circuit is shown in Fig. 17(b).

As shown in Fig. 17(b), the H-shaped HVDC network is equivalent to two point-to-point HVDC links with an ac equivalent tie line. The equivalent circuit of the H-shaped HVDC is shown in Fig. 18(a). Applying the $\Delta - \mathrm{Y}$ transform, the equivalent circuit of the integrated ac/dc system is converted to the circuit shown in Fig. 18(b). The impedances of the Y circuit are

$$\mathbf{Z}_{\mathrm{x}} = \frac{\mathbf{Z}_{1\_2} * \mathbf{Z}_{\mathrm{E}1\_1}}{\mathbf{Z}_{1\_2} + \mathbf{Z}_{\mathrm{E}1\_1} + \mathbf{Z}_{\mathrm{E}1\_2}} \mathbf{Z}_{\mathrm{y}} = \frac{\mathbf{Z}_{1\_2} * \mathbf{Z}_{\mathrm{E}1\_2}}{\mathbf{Z}_{1\_2} + \mathbf{Z}_{\mathrm{E}1\_1} + \mathbf{Z}_{\mathrm{E}1\_2}}$$
$$\mathbf{Z}_{\mathrm{z}} = \frac{\mathbf{Z}_{\mathrm{E}1\_1} * \mathbf{Z}_{\mathrm{E}1\_2}}{\mathbf{Z}_{1\_2} + \mathbf{Z}_{\mathrm{E}1\_1} + \mathbf{Z}_{\mathrm{E}1\_2}}. \tag{15}$$

The impedance of the equivalent tie line $\mathbf{Z}_{1\_2}$ needs to be small due to the limited power shift between two point-to-point VSC-HVDC links. Compared with $\mathbf{Z}_{1\_2}$, the equivalent impedances $\mathbf{Z}_{\mathrm{E}1\_1}$ and $\mathbf{Z}_{\mathrm{E}1\_2}$ can be much larger according to the expression of $\mathbf{Z}_{\mathrm{E}1}$ in (6). This results in the impedances $\mathbf{Z}_{\mathrm{x}}$ and $\mathbf{Z}_{\mathrm{y}}$ being much smaller than $\mathbf{Z}_{\mathrm{z}}$ in the Y-connection circuit. Therefore, the branch $\mathbf{Z}_{\mathrm{z}}$ can be moved downward for simplification, as shown in Fig. 19.

Voltage and current phasors of each VSC ac terminal can be obtained in real-time based on the PMU measurements. The four variables in Fig. 19 can be determined by

$$\mathbf{Z}_{\mathrm{E}2\_1} = \frac{\mathbf{V}_1 - \mathbf{V}_2}{\mathbf{I}_2}, \quad \mathbf{Z}_{\mathrm{E}2\_2} = \frac{\mathbf{V}_3 - \mathbf{V}_4}{\mathbf{I}_4},$$
$$\mathbf{Z}_{\mathrm{a}} = \frac{\mathbf{V}_1 - \mathbf{V}_3}{\mathbf{I}_1 - \mathbf{I}_2}, \quad \mathbf{Z}_{\mathrm{z}} = \frac{\mathbf{V}_3}{\mathbf{I}_1 - \mathbf{I}_2 + \mathbf{I}_3 - \mathbf{I}_4}. \tag{16}$$

Similar to the point-to-point case, the multi-HVDC equivalent circuit is also intended for long-term stability analysis and not for applications in electromagnetic time scales.

TABLE III
PARAMETERS OF 5-MW DFIG

Parameters	Values
Stator Resistance	0.003 p.u.
Stator Reactance	0.125 p.u.
Magnetizing Reactance	2.5 p.u.
Rotor Resistance	0.004 p.u.
Rotor Reactance	0.05 p.u.
Acceleration Time Constant	0.5 s

B. DFIG Parameters

The parameters of DFIGs are shown in Table III.

REFERENCES

[1] K. Bell, D. Cirio, A. M. Denis, L. He, C.-C. Liu, C. Moreira, and P. Panciatici, "Economic and technical criteria for designing future offshore HVDC grids," in *Proc. 2010 Europe IEEE PES Innovative Smart Grid Technologies (ISGT Europe)*, Gothenburg, Sweden, Oct. 2010.
[2] N. Flourentzou, V. G. Agelidis, and G. D. Demetriades, "VSC-based HVDC power transmission systems: An overview," *IEEE Trans. Power Electron.*, vol. 24, no. 3, pp. 592–602, Mar. 2009.
[3] A. M. Abbas and P. W. Lehn, "PWM based VSC-HVDC systems—A review," in *Proc. 2009 IEEE PES General Meeting*, Jul. 2009, pp. 1–8.
[4] L. Hu, "Sequence impedance and equivalent circuit of HVDC system," *IEEE Trans. Power Syst.*, vol. 13, no. 2, pp. 354–360, May 1998.
[5] A. Pizano-Martinez, C. R. Fuerte-Esquivel, H. Ambriz-Perez, and E. Acha, "Modeling of VSC-based HVDC systems for a Newton-Raphson algorithm," *IEEE Trans. Power Syst.*, vol. 22, no. 4, pp. 1794–1803, Nov. 2007.
[6] U. N. Gnanarathna, A. M. Gole, and R. P. Jayasinghe, "Efficient modeling of modular multilevel HVDC converters (MMC) on electromagnetic transient simulation programs," *IEEE Trans. Power Del.*, vol. 26, no. 1, pp. 316–324, Jan. 2011.
[7] M. Sultan, J. Reeve, and R. Adapa, "Combined transient and dynamic analysis of HVDC and FACTS systems," *IEEE Trans. Power Del.*, vol. 13, no. 4, pp. 1271–1277, Oct. 1998.
[8] A. Yazdani and R. Iravani, "Dynamic model and control of the NPC-based back-to-back HVDC system," *IEEE Trans. Power Del.*, vol. 21, no. 1, pp. 414–424, Jan. 2006.
[9] S. Cole, J. Beerten, and R. Belmans, "Generalized dynamic VSC MTDC model for power system stability studies," *IEEE Trans. Power Syst.*, vol. 25, no. 3, pp. 1655–1662, Aug. 2010.
[10] L. Tang and B.-T. Ooi, "Locating and isolating dc faults in multi-terminal dc systems," *IEEE Trans. Power Del.*, vol. 22, no. 3, pp. 1877–1884, Jul. 2007.
[11] M.-E. Grenier, N. Lefebvre, and T. V. Cutsem, "Quasi steady-state models for long-term voltage and frequency dynamics simulation," in *Proc. 2005 IEEE Power Tech Russia*, Jun. 2005, pp. 1–8.
[12] T. V. Cutsem, J. Kabouris, G. Christoforidis, and C. D. Vournas, "Application of real-time voltage security assessment to the Hellenic interconnected system," *Proc. Inst. Elect. Eng., Gen., Transm., Distrib.*, vol. 152, no. 1, pp. 123–131, Jan. 2005.
[13] M. Glavic and T. V. Cutsem, "A short survey of methods for voltage instability detection," in *Proc. 2011 IEEE PES General Meeting*, Jul. 24–29, 2011, pp. 1–8.
[14] K. Vu, M. M. Begovic, D. Novosel, and M. M. Saha, "Use of local measurements to estimate voltage-stability margin," *IEEE Trans. Power Syst.*, vol. 14, no. 3, pp. 1029–1035, Aug. 1999.
[15] S. Corsi and N. Taranto, "A real-time voltage instability identification algorithm based on local phasor measurements," *IEEE Trans. Power Syst.*, vol. 23, no. 3, pp. 1271–1279, Aug. 2008.
[16] M. Zima, M. Lasson, P. Korba, C. Rehtanz, and G. Andersson, "Design aspects for wide-area monitoring and control systems," *Proc. IEEE*, vol. 93, no. 5, pp. 980–996, May 2005.
[17] L. Xu, L. Yao, and C. Sasse, "Grid integration of large DFIG-based wind farms using VSC transmission," *IEEE Trans. Power Syst.*, vol. 22, no. 3, pp. 976–984, Aug. 2007.
[18] P. Kundur, *Power System Stability and Control*. New York, NY, USA: McGraw-Hill, 1994.
[19] C. W. Taylor, "Wide-area stability controls," in *Presented in Imperial College*, London, U.K., Mar. 2006.
[20] J. G. Slootweg and W. L. Kling, "Aggregated modelling of wind parks in power system dynamics simulations," in *Proc. IEEE Power Tech Conf.*, 2003, vol. 3, pp. 626–631.
[21] S. Li, Z. Liu, and Y. Jia, "Dynamic aggregation of doubly-fed induction generators (DFIGs) for stability analysis of wind power systems," in *Proc. 2011 IEEE PES General Meeting*, Jul. 2011, pp. 1–6.
[22] A. Ellis and E. Muljadi, "Wind power plant representation in large-scale power flow simulations in WECC," in *Proc. 2008 IEEE PES General Meeting-Conversion and Delivery of Electrical Energy in the 21st Century*, Jul. 2008, pp. 1–6.
[23] Y. Lei, A. Mullane, G. Lightbody, and R. Yacamini, "Modeling of the wind turbine with a doubly fed induction generator for grid integration studies," *IEEE Trans. Energy Convers.*, vol. 21, no. 1, pp. 257–264, Mar. 2006.
[24] P. Kundur *et al.*, "Definition and classification of power system stability," *IEEE Trans. Power Syst.*, vol. 19, no. 2, pp. 1387–1401, May 2004.
[25] L. Liao, "Fault location for single-circuit line based on bus-Zbus utilizing voltage measurements," *IEEE Trans. Power Del.*, vol. 23, no. 2, pp. 609–617, Apr. 2008.
[26] M. Nunes, J. Lopes, H. Zurn, U. Bezerra, and R. Almeida, "Influence of the variable-speed wind generators in transient stability margin of the conventional generators integrated in electrical grids," *IEEE Trans. Energy Convers.*, vol. 19, no. 4, pp. 692–700, Dec. 2004.
[27] D. J. Hill, "Nonlinear dynamic load models with recovery for voltage stability studies," *IEEE Trans. Power Syst.*, vol. 8, no. 1, pp. 166–176, Feb. 1993.

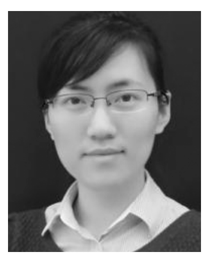

Lina He (S'11) received the B.S. and M.S. degrees from Huazhong University of Science and Technology, China, in 2007 and 2009, respectively. She is pursuing the Ph.D. degree in electrical engineering at University College Dublin, Ireland.

She was an Electrical Engineer at Tianjin Electric Power Corporation, State Grid, China, during 2009–2010. Her research interests include system security and protection coordination of ac grids with renewable energy integration, HVDC control and operation, and wide area protection.

Chen-Ching Liu (F'94) received the Ph.D. degree from the University of California, Berkeley, CA, USA.

He is presently Boeing Distinguished Professor at Washington State University, Pullman, WA, USA, and Professor of Power Systems at University College Dublin, Ireland. He was Palmer Chair Professor of Electrical Engineering at Iowa State University, Ames, IA, USA, and a Professor of Electrical Engineering at the University of Washington, Seattle, WA, USA.

Dr. Liu received an IEEE Third Millennium Medal in 2000 and the IEEE Power and Energy Society Outstanding Power Engineering Educator Award in 2004. He was recognized with a Doctor Honoris Causa from University Politehnica of Bucharest, Romania, in 2013.